



**Mechanism of Molecular Interaction of Acrylate-  
Polyethylene Glycol Acrylate Copolymers with Calcium  
Silicate Hydrate Surfaces**

Journal:	<i>Green Chemistry</i>
Manuscript ID	GC-ART-09-2019-003287.R1
Article Type:	Paper
Date Submitted by the Author:	01-Dec-2019
Complete List of Authors:	Jamil, Tariq; University of Colorado Boulder, Department of Chemical and Biological Engineering Javadi, Ali; Univ Akron, Dept Polymer Engn Heinz, Hendrik; University of Colorado-Boulder, Chemical and Biological Engineering

# **Mechanism of Molecular Interaction of Acrylate-Polyethylene Glycol Acrylate Copolymers with Calcium Silicate Hydrate Surfaces**

Tariq Jamil,<sup>1</sup> Ali Javadi,<sup>2</sup> Hendrik Heinz<sup>1\*</sup>

<sup>1</sup>Department of Chemical and Biological Engineering, University of Colorado-Boulder, Boulder,  
Colorado 80309, USA

<sup>2</sup>Department of Polymer Engineering, University of Akron, Akron, Ohio 44325, USA

\* Corresponding author: [hendrik.heinz@colorado.edu](mailto:hendrik.heinz@colorado.edu)

## Abstract

Obtaining insights into the adsorption and assembly of polyelectrolytes on chemically variable calcium silicate hydrate (C-S-H) surfaces at the atomic scale has been a longstanding challenge in the chemistry of sustainable building materials and mineral-polymer interactions. Specifically, polycarboxylate ethers (PCEs) based on acrylate and poly(ethylene glycol) acrylate co-monomers are widely used to engineer the fluidity and hydration of cement and play an important role in the search for building materials with a lower carbon footprint. We report the first systematic study of PCE interactions with C-S-H surfaces at the molecular level using simulations at single molecule coverage and comparisons to experimental data. The mechanism of adsorption of the ionic polymers is a two-step process with initial cation adsorption that reverses the mineral surface charge, followed by adsorption of the polymer backbone through ion pairing. Free energies of binding are tunable in a wide range of 0 to -5 kcal per mol acrylate monomer. Polymer attraction increases for higher calcium-to-silicate ratio of the mineral and higher pH value in solution, and varies significantly with PCE composition. Thereby, successive negatively charged carboxylate groups along the backbone induce conformation strain and local detachment from the surface. Polyethylene glycol (PEG) side chains in the copolymers avoid contact with the C-S-H surfaces. The results guide in the rational design of adsorption strength and conformations of the comb copolymers, and lay the groundwork to explore the vast phase space of C-S-H compositions, surface morphologies, electrolyte conditions, and PCE films of variable surface coverage. Chemically similar minerals and copolymers also find applications for other structural and biomimetic materials.

## Introduction

Concrete is the world's most abundant building material and consists of cement mixed with sand, water, and, most often, polymer additives.<sup>1-3</sup> Cement is made by heating a mixture of limestone ( $\text{CaCO}_3$ ), clay, and other compounds in a kiln to form calcium silicate and calcium aluminate phases.<sup>3</sup> Thereby, thermal elimination of  $\text{CO}_2$  causes major greenhouse gas emissions (>50%), along with burning of fossil fuels to heat kilns and operation of ball mills for grinding of the raw cement clinker into micrometer sized cement particles.<sup>4</sup> Overall, cement production accounts for 5% to 7% of the global carbon dioxide footprint,<sup>5</sup> and one possible pathway to reduce  $\text{CO}_2$  pollution may be the partial replacement of clinker with supplementary cementitious materials such as fly ash, slag, silica fumes, calcined clay, and natural pozzolans in so-called blended cements.<sup>6-8</sup> The exploration of such new materials benefits from understanding of the physical and chemical processes upon hydration of cement phases from the molecular scale which, in spite of many studies, remain fundamentally unclear.

The properties of cement depend substantially on organic additives supplied in solution, often called superplasticizers, that control workability (rheology), setting behavior, and contribute to the ultimate mechanical properties of concrete.<sup>1, 9-11</sup> The interaction of such polyelectrolytes with oxide and hydroxide particles is not well understood and benefits from insights down to the molecular scale to customize the properties of concrete.<sup>12-14</sup> Understanding such interactions also supports the development of functional bioinspired material structures, catalysts, hydrogels, and nanoparticle-based therapeutics.<sup>15, 16</sup>

The development of novel, greener cements aims at retaining favorable hydration, setting, and mechanical properties. The typical hydration kinetics of cement minerals involves several stages<sup>1, 3</sup> wherein the organic modifiers enable an increase of the fluidity of the cement paste and allow

processing at lower water-to-cement ratios. Reduced water content increases the early strength of concrete, reduces the porosity, and can enhance the late strength (in ordinary Portland cement). Common organic modifiers include copolymers of acrylate and polyethylene glycol-modified acrylate, called in short polycarboxylate ethers (PCEs) (Figure 1a, b). There is consensus that negatively charged polymer backbones, i.e., acrylate or methacrylate groups, adsorb on the mineral surfaces and neutral side chains such as polyethylene glycol (PEG) help prevent agglomeration of mineral particles, possibly by steric hindrance.<sup>12-14</sup> Ion pairing mechanisms have been suggested, however, underlying simulations exclude chemical details of the polymers, of the silicate mineral surfaces, and the electrolytes.<sup>17, 18</sup> Measurements of cement paste properties leave many open questions about the working mechanism,<sup>1, 11, 19</sup> and PCEs also affect the reactions at solid-liquid interfaces.<sup>20-22</sup> For example, the number density and length of side chains of the PCE comb-copolymers affect the retardation of the hydration reaction and mechanical properties of concrete.<sup>22-25</sup> Proposed correlations with polymer structure<sup>12, 13, 22, 25-28</sup> have remained difficult to verify due to the lack of control over grafting density and polydispersity of the molecular weight of PCEs. Based on current understanding, the role of C-S-H surface chemistry and morphology, the magnitude of molecular-level interactions of the polymer with the surface, and understanding of adsorbed conformations remain elusive.

To overcome these limitations, we identified the mechanisms of adsorption of PCE molecules on calcium silicate hydrate surfaces in aqueous solution using molecular simulations in full chemical resolution.<sup>29-31</sup> We employed a series of 9 polymers of variable molecular architecture (Figure 1a, b), reproducible surface models of calcium silicate hydrates (Figure 1c-e),<sup>32</sup> explicit solvent molecules, and utilized the Interface force field (IFF) which has been thoroughly validated for interfacial properties.<sup>31</sup> The calcium-silicate-hydrate surfaces were represented by three

different (h k l) surfaces of tobermorite  $14 \text{ \AA}$ ,<sup>33</sup> the closest well-known crystal structure to semi-ordered C-S-H gels (Figure 1c-e). For simplicity, we neglect additional pore electrolytes in the aqueous solution and maintain a constant low PCE surface coverage of 35%. The Interface force field (IFF) and the associated surface model database<sup>31</sup> realistically represent calcium silicate hydrate surface chemistry and interaction parameters.<sup>34, 35</sup> IFF consistently captures chemical bonding and internal polarity and covers cement minerals, silica, clays and other compounds, including pH-dependent surface chemistry and organic molecules such as PEG.<sup>29, 31, 36-39</sup> Computed surface, interfacial and mechanical properties are up to two orders of magnitude more accurate compared to alternative models<sup>40-43</sup> and were recently surveyed in comparison with several cement force fields (CemFF).<sup>32</sup> IFF models previously helped identify the working mechanism of organic additives during grinding of cement particles,<sup>44-46</sup> pH-dependent retardation of cement hydration in the presence of aluminate ions,<sup>35</sup> as well as mechanisms of crystal growth and catalytic activity.<sup>14, 31, 34, 36, 37, 47-49</sup>

Prior simulations of PCE adsorption on C-S-H surfaces have not been reported. Earlier atomistic simulations of PCEs have been carried out in solution<sup>30, 50, 51</sup> as well as in aqueous environment on  $\text{MgO}$ <sup>52</sup> and  $\text{C}_3\text{S}$ <sup>53</sup> surfaces. Simulations of simpler polymers on C-S-H surfaces have been reported (1.3 C/S ratio)<sup>40</sup> using force fields<sup>43</sup> that have large errors in surface energies due to unrealistic atomic charges.<sup>42</sup> Prior related studies also include coarse-grain simulations of polymers and charged disks<sup>54</sup> to rationalize the assembly of C-S-H crystals at the mesoscale.<sup>55</sup>

While reliable force fields have become available,<sup>31, 32</sup> however, current techniques cannot simulate real cement conditions due to limitations in length and time scale. Therefore, the choice of appropriate model systems, approximations, and awareness about limitations is critical. The primary constituents of early-stage hydrated cement are hydrated tricalcium silicate ( $\text{C}_3\text{S}$ ) and

hydrated tricalcium aluminate ( $C_3A$ ), of which the aluminate phases hydrate quickly. Calcium silicate hydrates (C-S-H) precipitate as a complex semi-amorphous gel with locally ordered and globally disordered morphology after longer periods of time. Modeling such C-S-H nanostructures is challenging as sampling over a large number of calcium-to-silicate (C/S) ratios, morphologies, water content, and electrolyte conditions is ideally required. IFF contains a C-S-H model builder,<sup>56</sup> yet the C-S-H design space is too large to be covered in a single study, especially when paired with a library of polymer compositions. In addition, experimental measurements may not be feasible for highly customized C-S-H models. We therefore postpone the use of customized C-S-H models and chose more reproducible surface models for this first systematic computational study of PCE adsorption mechanisms. Tobermorite 14 Å ( $Ca_5Si_6O_{16}(OH)_2 \cdot 7 H_2O$ ) is the closest regular, crystalline model compound for hydrated C-S-H surfaces.<sup>33</sup> The (001), (100), and (004) surfaces (Figure 1c-e) can be obtained in experiments, which may allow future experimental validation of the results, similar to testing of peptide binding on different silica surfaces previously.<sup>36, 37, 57</sup> The three tobermorite 14 Å surfaces display a range of area densities of  $Ca^{2+}$  ions, C/S ratios, silanol and siloxide groups, as well as calcium-to-water (C/H) ratios that represent possible C/S ratios of amorphous or semi-ordered C-S-H surfaces (Figure 1c-h). Along with the 9 single PCE oligomers of different composition (Figure 1a, b), we examined 27 different combinations of PCE comb copolymers and well-defined C-S-H surfaces. The size of the all-atom model systems was 10 to 20 nm. A color code represents different fractions of side chains in the oligomers (Figure 1b). We further assume aqueous interfaces without the addition of electrolytes other than the ions dissociated from the (h k l) tobermorite 14 Å surfaces, as well as calcium ions and acrylate ions from the PCEs in solution. Our model conditions correspond to the addition of PCE in acid form, which reacts with calcium hydroxide in the pore solution to form calcium salts of the PCE and

water. The possible wide range of electrolytes in pore solutions of cement such as  $\text{Na}^+$ ,  $\text{K}^+$ ,  $\text{Ca}^{2+}$ ,  $\text{SO}_4^{2-}$ ,  $\text{OH}^-$ , aluminate,  $\text{Mg}^{2+}$ , and  $\text{Cl}^-$  ions with concentrations between 0.0 and 0.2 M was not considered.<sup>58,59</sup> The surface coverage of single PCE molecules of 35% equals a comparatively low dosage of  $\sim 0.4$  mg PCE per 1 g of cement, which is about  $\sim 10\%$  of that in typical cement formulations.<sup>11</sup> We believe that understanding at the single molecule level provides a foundation for explaining the assembly of more densely packed polymer films going forward. The simulation conditions were overall chosen for simplicity and reproducibility, including initial tests for 0.2 M added  $\text{Ca}(\text{OH})_2$  and higher PCE surface coverage.

The outline of the paper is as follows. First, we describe the characteristics of the C-S-H surface models and aqueous interfaces, the polymers and their conformation in solution, as well as the surface coverage in molecular detail. Then, we proceed with the discussion of the adsorption mechanism, binding energies and adsorbed conformations as a function of the fraction of side chains in the backbone and of the length of side chains, free energies of adsorption, the influence of added salts and higher surface coverage, as well as comparisons to experimental measurements. Conclusions are given at the end. Computational details (Section S1), supplementary figures, tables, text, animations, and models to reproduce the simulations are provided in the ESI.

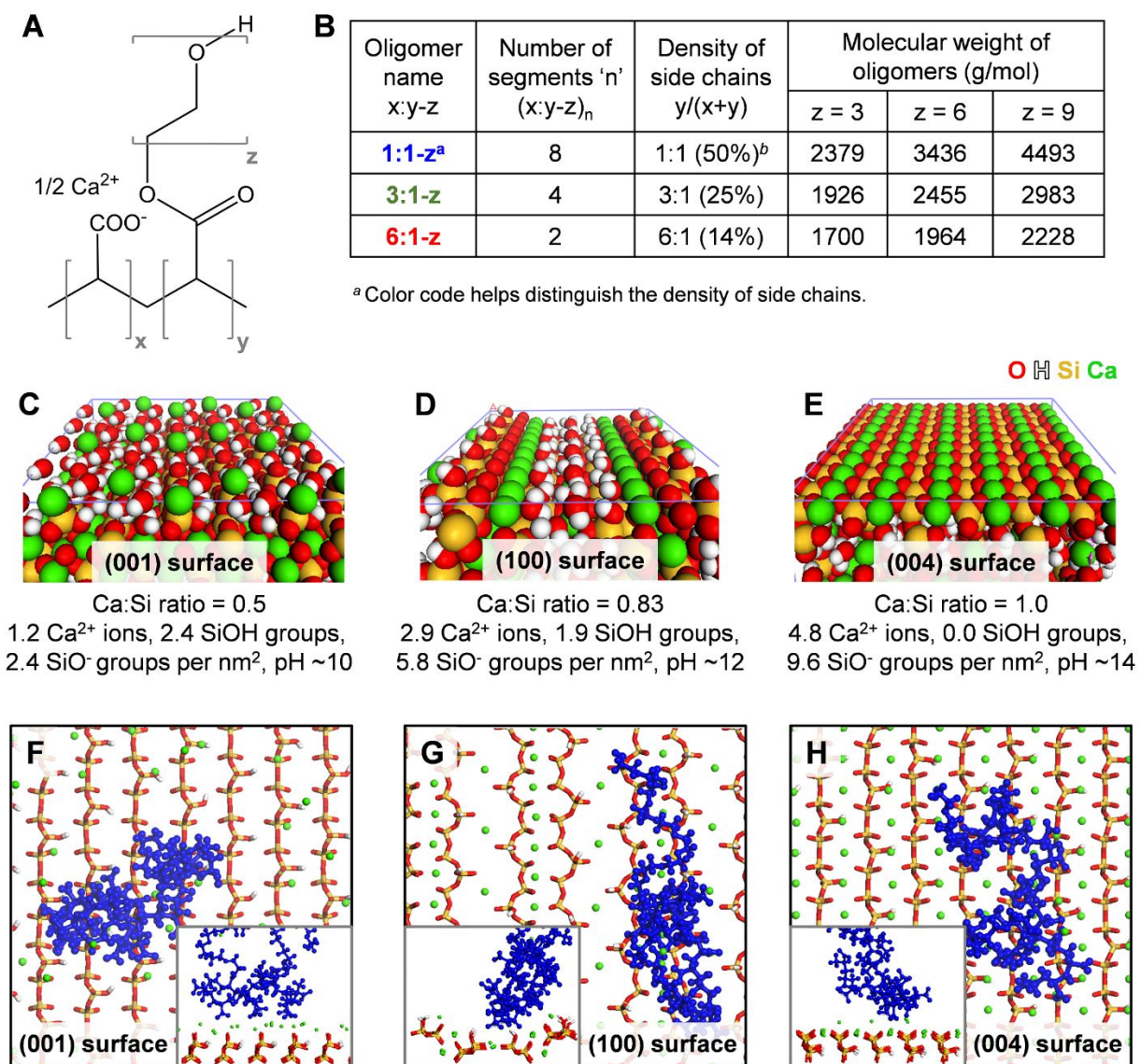


**Figure 1.** Structure of the acrylate-(polyethylene glycol)acrylate copolymers and tobermorite 14 Å surfaces that represent reproducible C-S-H surface environments. (a) Structural formula of the polymers, in short called polycarboxylate ethers (PCEs). (b) Abbreviation and molecular weight of the PCE models. The number of acrylate repeat units in all backbones is 16 ( $n \cdot (x + y) = 16$ ). (c-e) Side view onto the tobermorite 14 Å (001), (100), and (004) surfaces that represent C-S-H surfaces. Differences in surface chemistry are indicated by the specific Ca:Si ratios (C/S ratios), area densities of Ca<sup>2+</sup> ions, SiOH groups and SiO<sup>-</sup> groups, as well as approximate pH values

associated with these protonation states. (f-h) Top view onto the C-S-H model surfaces. The PCE 6:1-9 oligomer is shown on the surfaces at 35% surface coverage to indicate relative proportions. Only the first atomic layer of the calcium silicate surface is shown to visualize differences in the arrangement of silicate chains,  $\text{Ca}^{2+}$  ions, SiOH groups, and  $\text{SiO}^-$  groups. The insets show side views of the adsorbed polymers. 27 different polymer-surface combinations were tested (9 oligomers  $\times$  3 model C-S-H surfaces).

## Results and Discussion

**Models of the Tobermorite 14 Å Surfaces and Aqueous Interfaces.** The (001), (100) and (004) surfaces of tobermorite 14 Å exhibit an increase in the C/S ratio and in surface energy (= cleavage energy) (Figure 1c-e and Figure 2). The degree of ionization of surface silanol groups ( $\equiv\text{Si-OH}$ ) to siloxide groups ( $\equiv\text{Si-O}^-$ ) increases in the same order. Therewith, the solution pH value at which these surfaces are stable increases from pH  $\sim$ 10 to pH  $\sim$ 14. The correlation of solution pH with surface chemistry, i.e., different degrees of ionization, has been previously explained for silica surfaces<sup>37, 57</sup> and glasses<sup>60</sup> based on pK values for silicic acid and extensive laboratory data for surface titration.<sup>35, 57, 61, 62</sup> The representation of surface chemistry in C-S-H models in accordance with pH values in solution is essential to understand and predict interfacial properties, similar to other cement minerals,<sup>35, 62</sup> silica, and apatite surfaces.<sup>36, 63-65</sup> The chosen surface models of tobermorite 14 Å cover a typical range of surface chemistry in cement, corresponding to pH values between 10 and 14, and consist of connected silicate chains of three-mers (Dreierketten) (Figure 1c-h). The silicate chains assume regular orientations in the [010] direction on (001) and (004) surfaces (Figure 1c, e, f, h), as well as orientations in wide and small grooves on the periodic (100) surface (Figure 1d, g).

Molecular dynamics simulations were used to characterize the cleavage energy (= surface energy) and solid-water interfacial energies of these regular C-S-H surfaces (Figure 2). The (001) plane of tobermorite 14 Å is of lowest cleavage energy of  $\sim 380$  mJ/m<sup>2</sup>, followed by the (100) and (004) planes with an increase in surface energy to  $\sim 640$  mJ/m<sup>2</sup>. Cleavage of crystals preferably occurs along planes with rows of ions and avoids planes with polar covalent O-Si-O-Si-O bonds which requires multiple times more energy to break.<sup>47</sup> The (004) cleavage plane of tobermorite 14 Å (Figure 2a) is structurally equivalent to the (004) cleavage plane in tobermorite 11 Å (Merlino crystal structure) (Figure 2b),<sup>66</sup> where it is the cleavage plane of lowest energy (Figure 2d), and to the (002) plane in tobermorite 11 Å (Hamid crystal structure).<sup>67</sup> These cleavage surfaces can be obtained in experiment. In addition, the tobermorite-water interfacial energies for the chosen surfaces are in the range for voluntary hydration and wetting of -10 to +110 mJ/m<sup>2</sup> ( $\pm 20$  mJ/m<sup>2</sup>), similar to the surface tension of water of 72 mJ/m<sup>2</sup> or less.<sup>68</sup> The cleavage energies of the tobermorite surfaces are also much lower than in tricalcium silicate (C<sub>3</sub>S), which is the most abundant mineral phase before cement hydration and shows (hkl) cleavage energies in excess of  $\sim 1100$  mJ/m<sup>2</sup>.<sup>14</sup> The closest approximation for C-S-H surfaces formed upon hydration of Portland cement might be the (100) surface of tobermorite 14 Å with a surface C/S ratio of 0.83, equivalent to a bulk C/S ratio between 1.25 and 1.6. The (100) surface is expected to be stable at a pH value of  $\sim 12$ , which is similar to pore solutions with a pH value of  $\sim 13$ .<sup>35</sup>

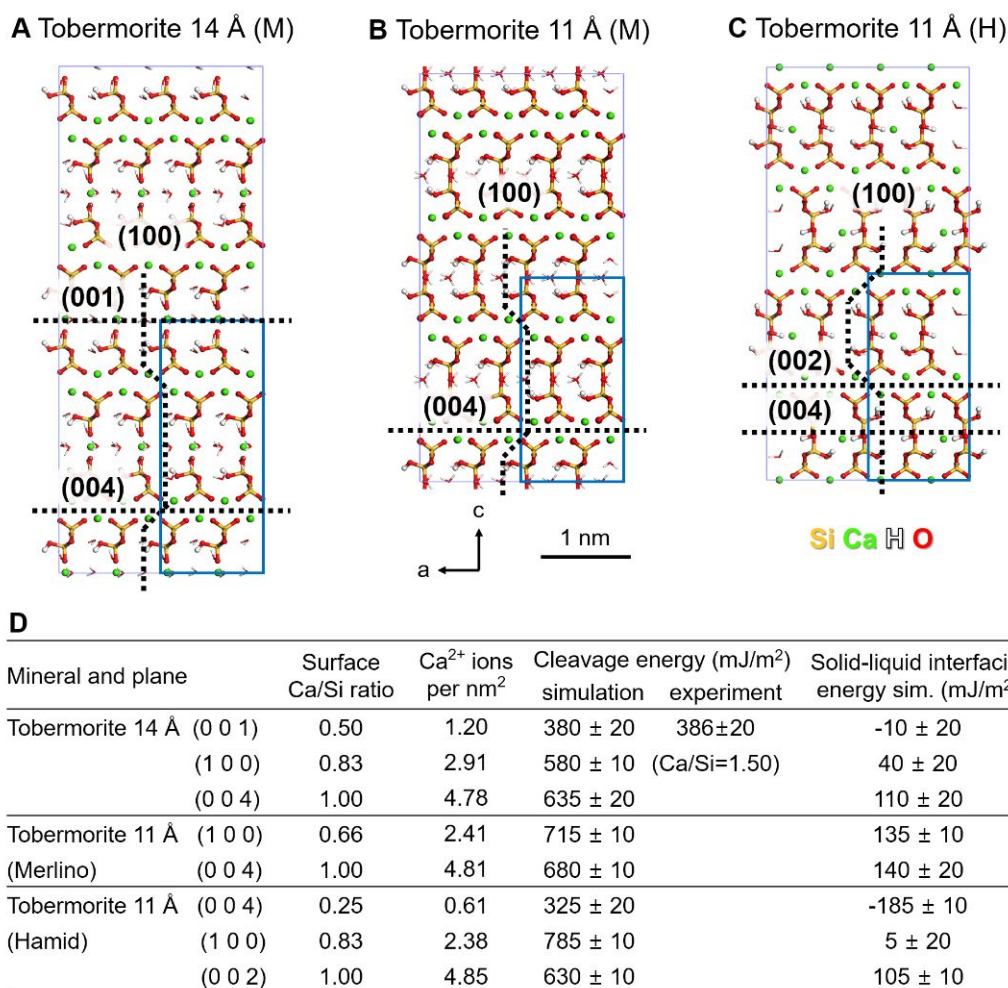


**Figure 2.** Structure and computed properties of low energy cleavage planes of tobermorite minerals. (a) Tobermorite 14 Å (refs. <sup>33</sup> and <sup>69</sup>). (b) Tobermorite 11 Å (Merlino, ref. <sup>66</sup>). (c) Tobermorite 11 Å (Hamid, ref. <sup>67</sup>). (d) Atomic-level structure of the surfaces and preferred cleavage planes. Dissection of polar covalent Si-O bonds is avoided and would increase cleavage energies by several 100 mJ/m<sup>2</sup>. (004) planes of tobermorite 14 Å are equivalent to (004) planes of tobermorite 11 Å (Merlino) and (002) planes of tobermorite 11 Å (Hamid). Solid-water interfacial energies on the order of 0 to 100 mJ/m<sup>2</sup> indicate hydration and compatibility with water. The average uncertainty is ±10 to ±20 mJ/m<sup>2</sup>.

Typical amorphous C-S-H surfaces in Portland cement consist of silicate chains that are further broken down into a distribution of short oligomers due to hydrolysis, and feature higher bulk C/S ratios of  $\sim 1.4$  to  $\sim 1.7$ . The C/S ratio in typical bulk C-S-H is significantly higher than in bulk tobermorite 14 Å, however, the C/S ratio on C-S-H surfaces and the exposed area density of  $\text{Ca}^{2+}$  ions remains similar to tobermorite 14 Å (h k l) surfaces. The similarity is due to exposure of less  $\text{Ca}^{2+}$  ions at C-S-H surfaces as a result of a more random three-dimensional distribution of  $\text{Ca}^{2+}$  ions in C-S-H. In contrast, the  $\text{Ca}^{2+}$  ions on the tobermorite 14 Å surfaces are concentrated in layers with higher area density than in the remaining volume of the mineral (Figure 2a). Accordingly, the tobermorite 14 Å (h k l) surfaces with bulk C/S ratios of 0.5 to 1.0 are reasonably representative of C-S-H surfaces with C/S ratios of 0.8 to 1.6. We accept a tradeoff between a wide range of amorphous C-S-H surfaces for the closely related, well-characterized tobermorite 14 Å (h k l) surfaces to enable reproducibility and future experimental verification.

We found that, on the (001), (100), and (004) tobermorite 14 Å surfaces, only between 3% and 0% of  $\text{Ca}^{2+}$  ions dissociate more than 3 Å away from superficial siloxide groups in aqueous solution (Figure 1c-e). In comparison to silica<sup>70, 71</sup> and clay mineral surfaces,<sup>63, 72</sup> this degree of dissociation is about one order of magnitude lower. The difference is related to the higher area density of negative charge at the elevated pH values and stronger localization of the negative charge on individual oxygen atoms (see further discussion in Section S2 of the ESI).

**Polymer Models and Conformations in Solution.** We utilized monodisperse models of the 9 different acrylate oligomers. All models have the same backbone length (16mer) of  $\sim 4.0$  nm in an extended conformation. In comparison to commercial PCEs with a backbone length of 50 to 60 units, the backbone length is only a fraction and chosen for computational feasibility.<sup>73</sup> The grafting density of PEG side chains was varied similar to prior experiments<sup>74</sup> at 50% (1:1-z), 25%

(3:1-z), and 14% (6:1-z), and the length of the side chains varied with  $z = 3, 6$  and  $9$  repeat units (Figure 1a, b). Commercial products often feature longer side chains, for example, 20 to 40 repeat units, and larger in some cases.

At the outset, the dynamics and conformations of the PCEs in the desorbed state are of interest as adsorption is driven by the differences in energies and free energies relative to the desorbed state. The anionic backbone and the PEG side chains are soluble in water. The equilibrium between extended and globule-like conformations is affected by the topology and the dynamics by the coordination of the  $\text{Ca}^{2+}$  ions to the carboxylate groups (Figure 3). A lower density of side chains, or shorter side chains, lead to more globular conformations and faster conformation changes between different states (Figure 3b, c, f, i, j). Neighboring  $\text{COO}^-$  groups in the backbone avoid close contacts with each other due to electrostatic repulsion and associated hydration shells. More direct contact of  $\text{Ca}^{2+}$  ions with the backbone is observed. In contrast, the acrylate backbone of PCEs with densely grafted and longer side chains tends to be rigid and extended in solution (Figure 3d, g, j). Then, the side chains diminish access of hydrated  $\text{Ca}^{2+}$  ions to the negatively charged backbone and favor a larger end-to-end length. The fraction of  $\text{Ca}^{2+}$  ions coordinated with the polymer backbone in solution amounts up to  $\sim 35\%$  in PCEs 1:1-z, up to  $\sim 50\%$  in PCEs 3:1-z, and up to  $\sim 75\%$  in PCEs 6:1-z. The calcium ions were hereby present in a stoichiometric amount to neutralize the negative charge on the acrylate backbone, without further addition of electrolytes such as  $\text{Ca}$ .

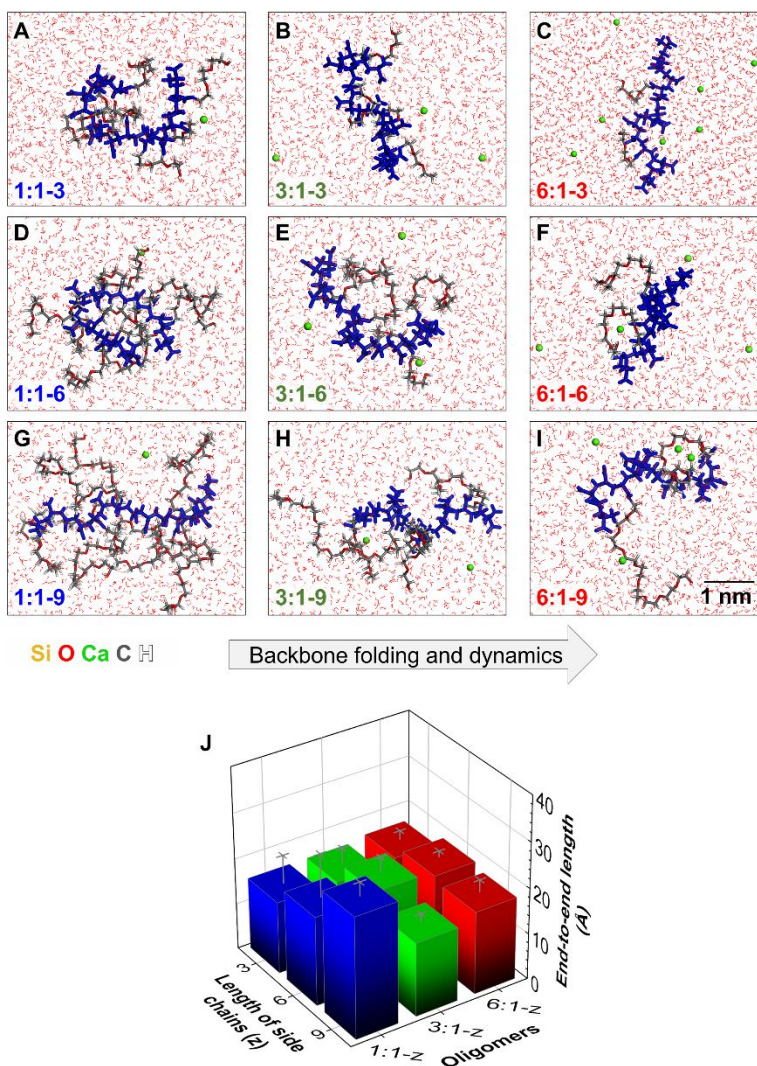


**Figure 3.** Equilibrium conformations of the 16-mer polycarboxylate ethers (PCEs) in dilute aqueous solution and end-to-end distance of the acrylate backbone. (a-c) PCEs with 3-mer side chains ( $z = 3$ ). (d-f) PCEs with 6-mer side chains ( $z = 6$ ). (g-i) PCEs with 9-mer side chains ( $z = 9$ ). The backbone is highlighted in dark blue. (j) Corresponding average end-to-end distances of the 16-mer acrylate backbone. From left to right, oligomers tend to assume more flexible, folded conformations due to lower amount of PEG side chains and a higher negative charge across the backbone. In the same order,  $\text{Ca}^{2+}$  ions bind more closely to acrylate anions in the backbone and accelerate conformation changes per unit time through variable coordination.

**Surface Coverage and Dosage in the Simulation in Comparison to Experiment.** The dimensions of the (hkl) tobermorite 14 Å surfaces for adsorption were designed to be between 3.4 x 3.7 nm<sup>2</sup> and 5.6 x 6.7 nm<sup>2</sup> so that extended, flat-on conformations of the PCEs consistently cover 35±3% of the surface area (Figure 1f-g, Table S1 and Section S1 in the ESI). The surface area covered in flat-on conformations is linearly proportional to the molecular weight of the polymer because the density of all PCEs is the same within few percent.

To understand the actual thickness of an adsorbed organic film, it is helpful to recall the thickness of a continuous single organic layer, such as a hydrocarbon chain or a PEG chain, of ~0.4 nm.<sup>75</sup> An ideal monolayer of this type requires ~1.2 mg PCE per 1 g of cement (assuming a specific surface area of cement of ~2 m<sup>2</sup>/g).<sup>11, 26</sup> To cover the entire particle surface in practice, however, more PCE is used as the molecules lack complete conformational flexibility and do not spread out in flat-on conformations of 0.4 nm thickness. The typical dosage of 2 to 8 mg PCE per 1 g of cement in concrete processing<sup>11</sup> thus generates continuous PCE films of 1 to 3 nm thickness that effectively assemble into multilayer structures. In contrast to such continuous polymer films, our first study in all-atom detail focuses on low, single molecule coverage at 35%. The mass dosage (in g PCE per g of cement mineral) was obtained from the surface coverage, converted into mass of the PCE molecule (in g) per surface area (in m<sup>2</sup>, see Table S1 in the ESI), multiplied by the specific surface area of cement (for example, ~2 m<sup>2</sup>/g in the dry or hydrated state).<sup>11, 26</sup> The dosage amounts to ~0.4 mg PCE per g of cement in our calculations. The interpretation of available experimental data takes the differences between model systems and laboratory systems into account.

**Adsorption Mechanism of the Comb Copolymers.** The common events in the binding mechanism of PCEs involve the initial migration of  $\text{Ca}^{2+}$  ions to the C-S-H surfaces (Figure 4a, b), followed by the anionic polymer backbone (Figure 4c), and conformation adjustments on the surface (Figure 4d). The first approach to the surface often occurs by an end of the polymer chain with successive  $\text{COO}^-$  groups and multiple negative charges (Figure 4e). The common occurrence of more than two successive carboxylate groups in the backbone of the PCEs results in local detachment from the surface owing to electrostatic repulsion and steric effects (see Movie S1 in the Supporting Information). Tilted and partially upright conformations can then result.

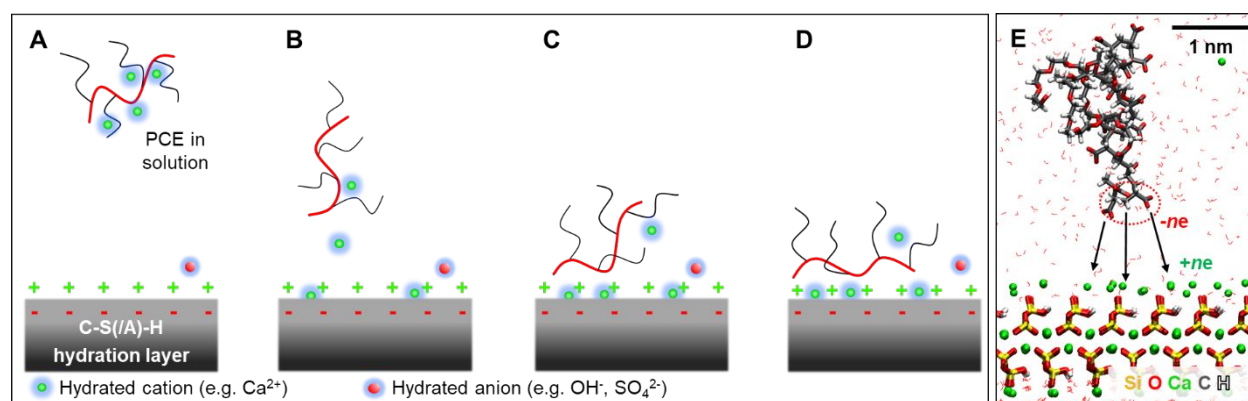


**Figure 4.** Sequence of events involved in the binding of PCEs to all C-S-H surfaces. (a) PCE molecules in solution more than 3 nm apart from the surface. (b) The conformation of the PCE changes during the approach to the surface. Calcium ions dissociate from the negatively charged acrylate backbone and bind to vacant surface sites. (c) The acrylate backbone follows the cations and initially binds to the C-S-H surface. (d) The PCE conformation adjusts depending on the structure of polymer x:1-z, the C-S-H surface chemistry, the pH value in solution, and the presence of additional ions (not shown). (e) Snapshot of a PCE backbone with a flexible end containing

multiple negatively charged  $\text{COO}^-$  groups, which move towards the surface and compete for superficial  $\text{Ca}^{2+}$  ions.

Hereby, the tobermorite  $14 \text{ \AA}$  (h k l) surfaces differ from the bulk mineral through the presence of vacant  $\text{Ca}^{2+}$  sites and under-coordinated siloxide groups ( $\equiv\text{SiO}^-$ ) to which the  $\text{Ca}^{2+}$  ions of the polymer are rapidly attracted (blue arrows in Figure 5b, e, h). These sites promote the initial dissociation of  $\text{Ca}^{2+}$  ions from the negatively charged PCE backbone and migration to the mineral surface (Figure 4a, b). Subsequent motion of the negatively charged bulky polymers to the surface and the formation of ion pairs between the  $\text{COO}^-$  groups of the polymer and  $\text{Ca}^{2+}$  ions on the mineral surface (Figure 4c, d and Movie S1 in the ESI) leads to a range of binding patterns and conformations. The preferred binding patterns and conformations depend on the mineral surface chemistry, the density of side chains (Figure 5) as well as the length of side chains (Figure 6). Full understanding of the atomic-level details requires side views (Figures 5 and 6, as well as Figure S1 in the ESI) and top views (Figure 1f-h and Figures S2 to S4 in the ESI). Moreover, representative 3D models are supplied in the ESI. A first measure to assess binding of the oligomers to the C-S-H surfaces was the contact time. The contact time was defined as the percentage of total simulation time during which any atoms of the PCE were within 1.0 nm distance from oxygen atoms in the top atomic layer of the C-S-H surface as an average over multiple replicas. The contact cutoff distance was chosen larger than usual (0.3 nm)<sup>73, 76, 77</sup> as some PCEs showed steady binding at several Angstrom distance from the surface (PCEs 1:1-9 and 1:1-6 on (001) and (004) surfaces, see section S1.5 in the ESI for details).

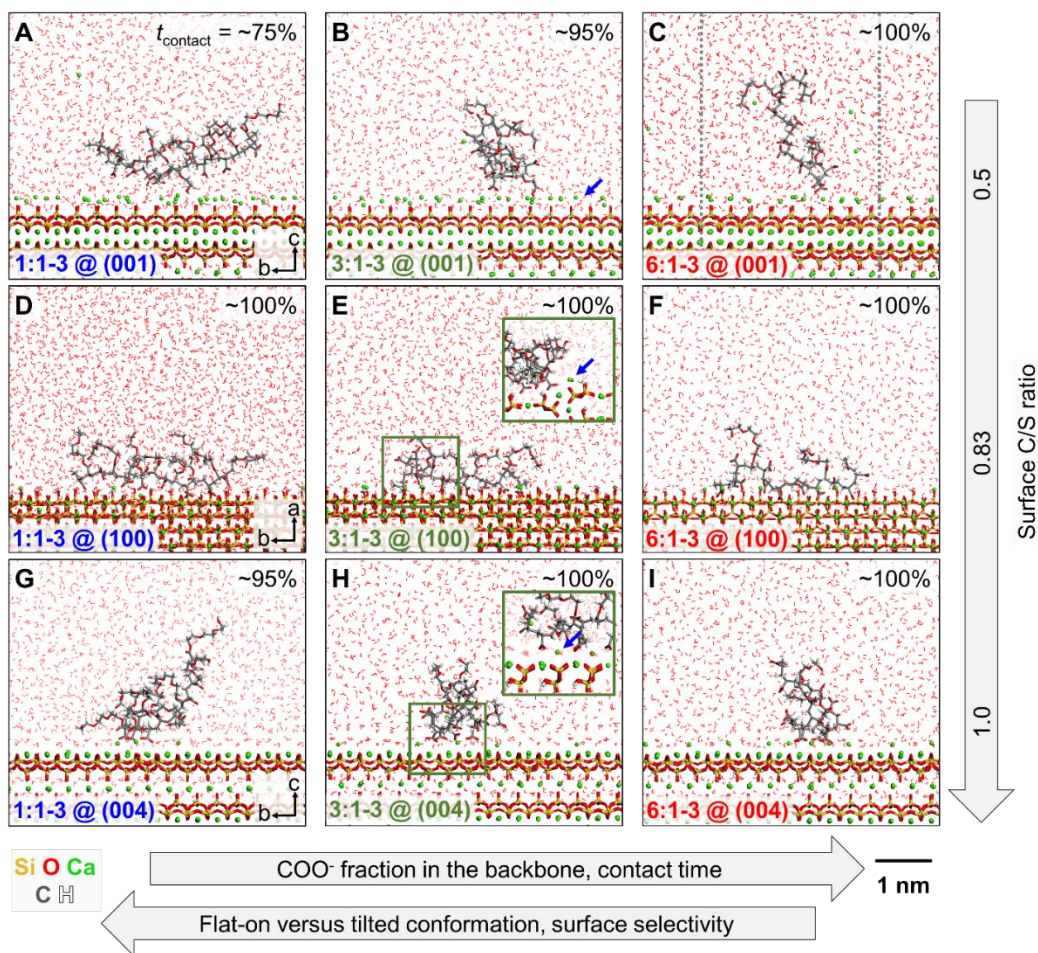


**Figure 5.** Interaction of PCEs with short side chains with the C-S-H model surfaces in side view. First,  $\text{Ca}^{2+}$  ions from the PCEs adsorb at available coordination sites of the cleavage plane (blue arrows in b, e, h) followed by ion pairing of the PCE backbone via acrylate side groups to calcium ions on the surface. (a-c) Representative conformations on the (001) surface of tobermorite 14 Å. Contact time with the surface via ionic side groups increases as the fraction of side chains decreases

(a to c). (d-f) Representative conformations on the (100) surface of tobermorite 14 Å. The binding strength is higher than on the (001) surface and the contact time  $\sim 100\%$ . (g-i) Representative snapshots on the (004) surface of tobermorite 14 Å. Binding is stronger than on the (001) surface but weaker than on the (100) surface. PCE binding is overall less dependent on the surface chemistry for a lower fraction of side PEG chains due to increased conformational flexibility and backbone ends rich in  $\text{COO}^-$  content (c, f, i). PCEs with a low fraction of side chains more frequently assume tilted and upward orientations relative to the surface (see panel (c) with periodic boundary condition shown as dotted lines). The height of the simulation boxes was greater than shown for clarity.

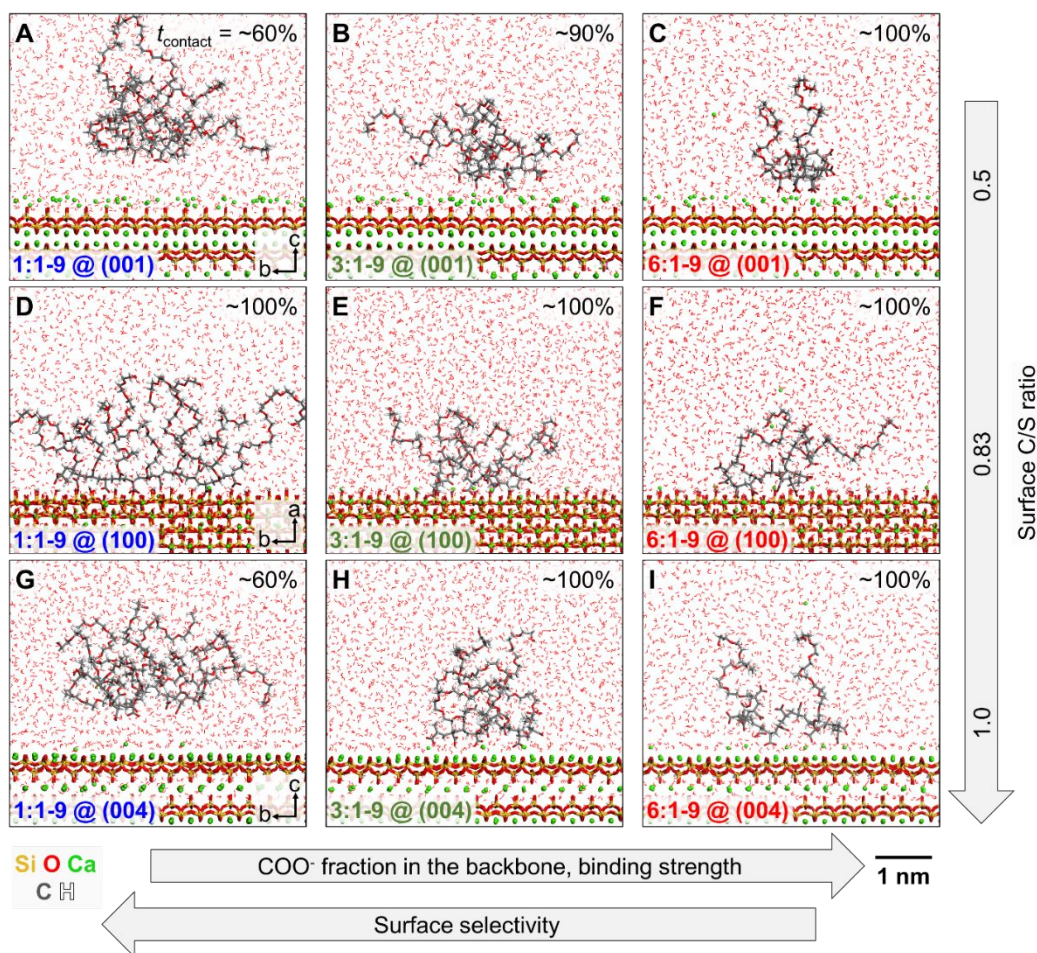


**Figure 6.** Interaction of PCEs with long side chains with the model C-S-H surfaces in side view. (a-c) Representative conformations and time in contact with the (001) surface of tobermorite 14 Å. The fraction of side chains decreases from (a) to (c) and leads to more contact time with the surface via ionic side groups. (d-f) Representative conformations on the (100) surface of tobermorite 14 Å. Binding is stronger than on (001) surfaces and contact times are 100%. (g-i) Representative conformations on the (004) surface of tobermorite 14 Å. The contact time, although not necessarily the binding strength, decreases relative to the same systems with shorter PEG side chains as access of COO<sup>-</sup> side groups to surface binding is diminished (a, b, g). The height of the original simulation boxes was greater than shown for clarity.

The major contribution to adsorption is the formation of SiO<sup>-</sup> ⋯ Ca<sup>2+</sup> and Ca<sup>2+</sup> ⋯ -OOC-R ion pairs which often assume distances less than 3 Å (Figure 7a).<sup>36, 37, 63</sup> In addition, on the (100) surface, adsorption is supported by multiple hydrogen bonds between surface silanol groups and acrylate anions in the polymer backbone (≡SiOH ⋯ -OOC-R) (Figure 7b). Nevertheless, a similar strength of these interfacial hydrogen bonds to hydrogen bonds with water molecules prior to adsorption preempts a significant contribution to adsorption. Silanol groups are also present on the (001) surface although they do not participate in hydrogen bonding due to their position 2 to 3 Å below the superficial layer of ≡SiO<sup>-</sup> groups and Ca<sup>2+</sup> ions and inaccessibility by the bulky carboxylate groups in the PCEs (Figure 1c, Figure 5a-c, Figure 6a-c, Figure S4a-c in the ESI). Hydrogen bonds can also form between alcohol-terminated PEG side chains (-OH) and surface siloxide groups (≡SiO<sup>-</sup> ⋯ HOR) on all C-S-H surfaces (Figure S5 in the ESI). Such hydrogen bonds can play a role relative to PCEs with methyl-terminated PEG side chains (-CH<sub>3</sub>), which cannot form such hydrogen bonds. The OH-terminated PCEs can maintain better surface contact

and enable the same fluidity of concrete paste at lower concentration.<sup>78, 79</sup> A notable contribution to adsorption of the backbone furthermore arises from conformation strain caused by more than two successive COO<sup>-</sup> groups, which tend to desorb from the surface and induce locally tilted or upright orientations (Figure 7c). Minor contributions to adsorption can also be associated with van der Waals interactions, which are similar before and after adsorption due to similar polarizability of the surrounding major atoms (Si, O, C, Ca).<sup>31</sup>

Polyethylene glycol (PEG) side chains avoid direct contact with the tobermorite surface in all 27 model systems (Figures 5, 6, and Figure S1 in the ESI). The oxygen atoms of PEG side chains in C–O–C bonds carry less negative charge (-0.40e) than oxygen atoms in water molecules (-0.82e). Smaller internal dipoles of the C–O–C bonds in PEG monomers in comparison to water molecules lead to less attraction to Ca<sup>2+</sup> ions and to SiO<sup>-</sup> ions on the mineral surface to form a solvation shell. Therefore, the loose PEG side chains prefer to stay in solution and show no affinity to the C-S-H surface, in contrast to the possible action as multidentate ligands for ions in circular crown ethers.<sup>80</sup>

The adsorption of Ca<sup>2+</sup> ions onto the overall electroneutral calcium-silicate-hydrate surfaces in this manner can explain neutralization, or reversal, of a negative zeta potential towards positive values as observed upon addition of PCEs in experiment.<sup>81</sup> Subsequent adsorption of excess carboxylate could also decrease the zeta potential to larger negative values,<sup>11, 82</sup> and both scenarios have been observed. In addition, analogous to the electrostatic repulsion between neighboring carboxylate groups (Figure 7c), repulsion between neighboring negatively charged disiloxide groups ( $-\text{SiO}_2^{2-} - \text{O} - \text{SiO}_2^{2-}$ ) can be observed in the silicate chains of the tobermorite surface (Figure 1f-h). The OSiO planes in each group bend apart by  $\sim 13^\circ$  and the third successive disiloxide group on bridging silicate tetrahedra points downwards to relax the strain.<sup>33</sup>

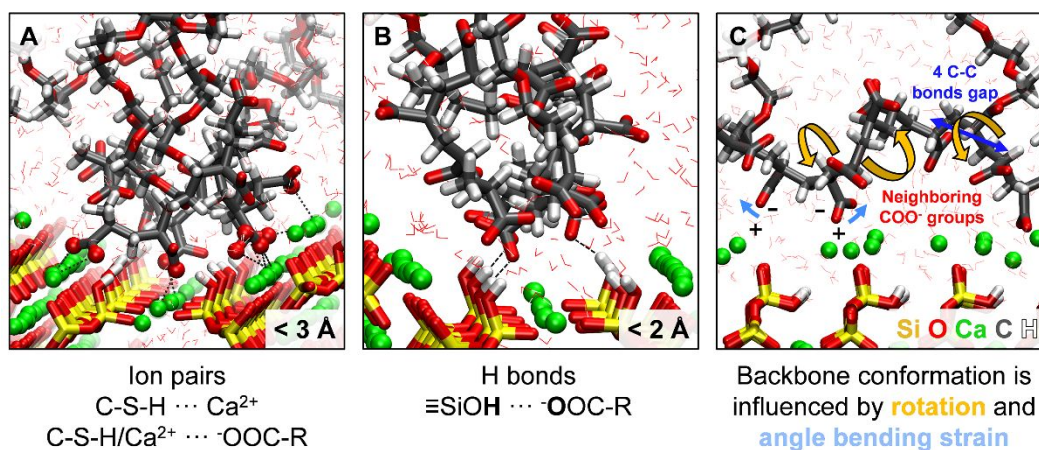


**Figure 7.** Main contributions to binding of polycarboxylate ethers onto the model C-S-H surfaces.

(a) Formation of ion pairs on the surface (shown for the (100) surface). (b) Hydrogen bonds between surface silanol groups and oxygen atoms in the carboxylate groups of the polymer backbone depending on the pH value in solution. (c) Conformation strain among consecutive COO<sup>-</sup> groups in the backbone due to competition for binding to Ca<sup>2+</sup> ions on the C-S-H surface. Angle bending (blue highlights) and rotational strain (orange highlights) force the polymer locally out of a flat-on orientation into tilted orientations when more than two successive COO<sup>-</sup> groups are present. A segment of four C-C bonds (2 monomers) between adjacent COO<sup>-</sup> groups by ester side chains can relieve the strain and support reorientation towards the surface (dark blue arrow, shown on the (001) surface).

**Binding Energy and Conformations.** All PCEs undergo exothermic adsorption. Binding energies range between -2 kcal/mol and -49 kcal/mol for the 16mer chains depending on the surface and the polymer (Figure 8a-c). The trends are similar when the adsorption energy is expressed per unit mass instead of per mole (in cal/g) (Figure S6 in the ESI). Energy and enthalpy

of binding are identical due to negligible volume work upon adsorption ( $<0.01$  kcal/mol). A major influence arises from the C/S ratio of the surface, and binding increases by more than three-fold from the (001) surface at pH  $\sim 10$  (Figure 8a) to the (100) surface at pH  $\sim 12$  (Figure 8b), and slightly further to the (004) surface at pH  $\sim 14$  (Figure 8c). The reason is the availability of more calcium ions per unit area for facile coordination of carboxylate groups from the PCE backbone. Thereby, high (Figure 8b and Figure 1d, g) and very high  $\text{Ca}^{2+}$  area density on the surface (Figure 8c and Figure 1e, h) lead to similar results, whereby the (004) surface allows more differentiation among polymer structures.

Another influence on binding strength is associated with the fraction and regularity of ester side chains (Figures 5, 6 and Figure S1 in the ESI). A lower fraction of side chains tends to support adsorption, such as in the 6:1-z and 3:1-z oligomers, which have more available  $\text{COO}^-$  groups for binding. In addition, longer side chains in these PCEs shield ionic interactions between adjacent polymer backbones and support stronger polymer-surface binding. The trend inverses for a high fraction of side chains in PCEs 1:1-z when longer, more densely packed side chains stiffen the backbone and reduce optimized contact between  $\text{COO}^-$  groups and calcium ions on the C-S-H surface (Figure 6a, d, g). The higher fraction of side chains in PCEs 1:1-z also introduces more surface-selective binding as seen by larger differences in adsorption enthalpy and larger differences in contact time on the different (hkl) surfaces compared to other polymers (Figure 8a-c as well as Figures 5, 6, and Figure S1 in the ESI). PCE 1:1-3 with short side chains shows strong binding comparable to PCEs 6:1-9 due to relatively high conformational flexibility. Many longer side chains such as in PCE 1:1-9 occupy a larger area to adsorb and have a larger excluded volume (Figure S4a, d, g in the ESI). The side chains then shield more potential binding sites on the surface that could otherwise be accessed by acrylate anions in the PCE backbone. Adsorption energies are

then reduced (Figure 8a-c) in agreement with experiments that report less PCE adsorption for increasing PEG content.<sup>26, 83</sup> The PCEs in near flat-on conformations also show an orientation preference parallel to the silicate chains on the tobermorite 14 Å surfaces (Figure 1g and Figures S2, S3, S4d-f in the ESI).

Furthermore, consecutive COO<sup>-</sup> groups along the PCE backbone (in PCEs 6:1-z and 3:1-z) have difficulty to bind to the pattern of Ca<sup>2+</sup> ions on the C-S-H surfaces due to electrostatic repulsion, angle bending strain, and rotation strain. These effects allow only up to two successive COO<sup>-</sup> groups in the PCE backbone to adsorb next to each other (Figure 7c). Three successive COO<sup>-</sup> groups were not found to adsorb in a row and force the backbone out of a flat-on conformation, often leading to tilted conformations (Movie S2 in the ESI). The presence of nonionic monomers with PEG side chains in between such carboxylate monomers helps relieve local conformation strain and extends surface contact (Figures 5d and 6d). As a rationale, energy barriers less than 1 kcal/mol are usually required for stretching of bond angles and rotation of (C–)C–C(–C) bonds in the polymer backbone according to experimental measurements.<sup>84, 85</sup> The computed binding energies of the PCEs are typically stronger, exceeding -1 kcal per mol of COO<sup>-</sup> groups or -16 kcal/mol per 16mer backbone (Figure 8a-c), and can thus trigger such conformational changes.

The foregoing observations are also backed up by the average end-to-end length of the oligomer backbone on the (001), (100), and (004) surfaces of tobermorite 14 Å (Figure 8d-f). Weaker adsorption tends to be accompanied by larger end-to-end length and thus higher backbone stiffness, and stronger adsorption is found for more flexible backbones with shorter end-to-end length. The maximum extended length is 40 Å and closely approached by PCEs 1:1-z on the (100) surface. The stiff 1:1-z backbone conformations parallel to the surface and higher end-to-end

length are assisted by the presence of side chains and the absence of neighboring  $\text{COO}^-$  groups. Extended conformations were also observed for PCE 6:1-3 (Figure 8d-f) and similarly reduce the binding strength (Figure 8a-c), although with a tilted backbone orientation relative to the surface, closer to upright orientation.

The density profiles of calcium ions on the tobermorite 14 Å surfaces and of oxygen atoms of carboxylate groups of the PCEs in contact with the surface consistently show a thicker layer of carboxylate groups for PCE 6:1-9 near the surface with more close contacts, a slightly weaker layer for PCE 3:1-9, and only a diffuse region for PCE 1:1-9 (Figure 8g). The amount of contact correlates with decreasing adsorption in this order (Figure 8a). The density profiles moreover indicate that calcium ions are highly concentrated at the surface ( $<3$  Å) and their number density is about an order of magnitude smaller in the region of bound polymer (Figure 8g). Details of the coordination of bound polymer to calcium ions are seen from the radial distribution function (RDF) of calcium ions and the oxygen atoms in  $\text{COO}^-$  groups of the PCE, which shows a maximum at 2.6 to 2.7 Å, indicative of the formation of  $\text{Ca}^{2+} \cdots \text{OOC}$  ion pairs at the surface (Figure 8h). The intensity of this peak decreases for polymers that are not in contact with the surface, and  $\text{Ca}^{2+}$  ions show no specific binding to PEG side chains.

Higher temperature during annealing (as described in Section S1 in the ESI) increased the surface contact time of all PCEs to near 100% regardless of the chemistry. This observation agrees with experimental observations of higher adsorbed mass at higher temperature.<sup>86, 87</sup> Effectively, higher temperature increases the mobility of water molecules in the simulation, leading to less water interaction with the surface and reinforcing polymer adsorption to calcium ions on the mineral surface. Further details on binding and adsorbed conformations are described in Section S3 in the ESI.

The binding mechanism and the binding energies reported were not dependent on the initial orientation of the PCE on the surface, which was verified by using between 5 and 10 replicas of different initial orientation and the resulting uncertainty (Figure 8a-c) (see Sections S1.3-S1.6, and S1.8 in the ESI).

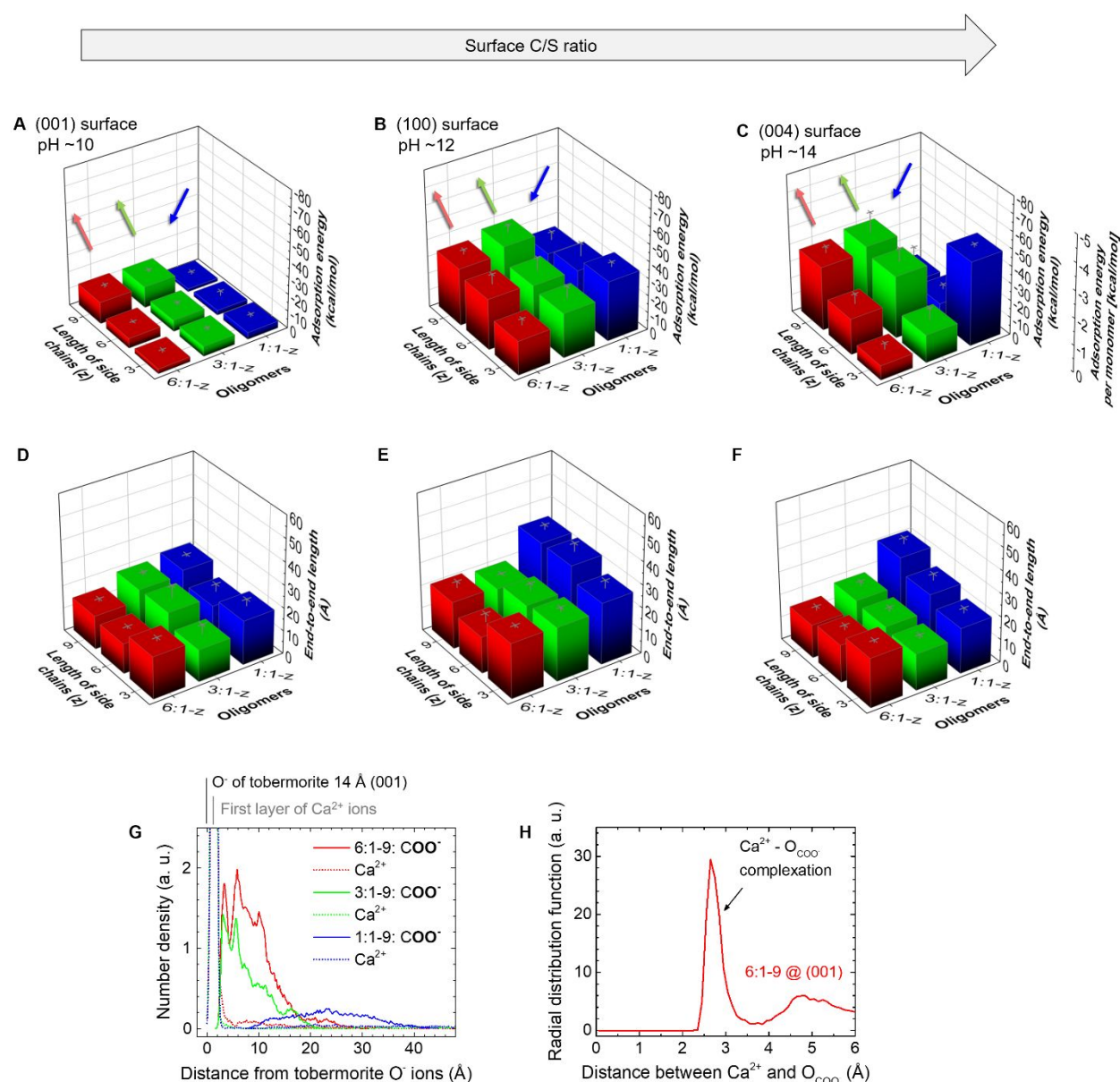


**Figure 8.** Adsorption energy and structural characteristics of the bound PCEs as a function of C-S-H surface chemistry and polymer structure and. (a-c) Adsorption energies on the (001), (100), and (004) surfaces of tobermorite 14 Å correlate with the extent of contact between COO<sup>-</sup> groups in the backbone and calcium ions on the surface. Adsorption tends to be stronger for a higher C/S ratio of the surface (a to c), as well as for a low fraction of side chains in PCEs 6:1-z and 3:1-z as there are many available COO<sup>-</sup> groups. Adsorption for the more ionic oligomers (6:1-z and 3:1-z) also increases towards longer side chains that help shield ionic interactions between adjacent polymer backbones and result in stronger polymer-surface binding. An opposite trend is observed for PCEs 1:1-z with a high fraction of side chains as longer, more densely packed side chains stiffen the backbone and diminish optimized contact between COO<sup>-</sup> groups and calcium ions on the C-S-H surface. (d-f) Average end-to-end length of the oligomer backbone on (001), (100), and (004) surfaces of tobermorite 14 Å. Larger end-to-end length corresponds to higher backbone stiffness and typically results in weaker adsorption, and vice versa. PCEs 1:1-z assume extended backbone conformations parallel to the surface, assisted by the side chains and the absence of neighboring COO<sup>-</sup> groups, and reach end-to-end lengths close to contour length of 40 Å on the (100) surface. Extended conformations for PCE 6:1-3 are associated with an orientation upward from the surface. (g) Density profile of calcium ions and oxygen atoms in carboxylate groups of PCEs x:1-9 on the (001) surface. A thicker surface-bound layer forms for PCE 6:1-9 due to the presence of more carboxylate groups and calcium ions, consistent with stronger adsorption. The trend is similar on the other (hkl) surfaces. (h) Radial distribution function of Ca<sup>2+</sup> ions, from the (001) surface and the PCE 6:1-9 combined, and the O atoms in the COO<sup>-</sup> groups in the PCE. The major peak at 2.6 Å distance originates mainly from the interaction of superficial Ca<sup>2+</sup> ions with the carboxylate group in the polymer backbone and is characteristic for bound conformations.

**Free Energy of Polymer Adsorption.** Steered molecular dynamics was used to probe the free energy of binding of the polycarboxylate ethers with side chains of 9 monomer length (PCE x:1-9) (Figure 9a-c).<sup>88, 89</sup> Hydrodynamic resistance (Figure 9d) from a pulling velocity applied to the center of the backbone (Figure 9e) was negligible. The trend in the free energy of binding (Figure 9a-c) is the same as for the energies of binding in all cases (Figure 8a-c). The free energies of adsorption tend to be the same as the adsorption energies within the uncertainty on (001) and (004) surfaces (Figure 9a, c), however, larger negative free energies are found for two of the three polymers on (100) surfaces (Figure 9b). Similarity in values indicates a small net entropy change upon adsorption, reminiscent of reports on peptide adsorption on silica and metal surfaces.<sup>36, 90</sup> The loss in polymer flexibility upon binding to the surface is then approximately offset by the gain in mobility of water molecules released from the surfaces. A significant entropy gain on the (100) surfaces by the more ionic PCEs 6:1-9 and 3:1-9 is associated with penetration of two distinct water layers and large gains in water mobility (Figure S7 in the ESI).

Nevertheless, the free energy data are qualitative as several of the  $\text{Ca}^{2+}$  ions that neutralize the negative charge on the polymer backbone remain bound on (001) and (004) surfaces, and nearly all such  $\text{Ca}^{2+}$  ions remain bound on the (100) surface. Therefore, the free energy curves exhibit a distance dependence beyond 2 to 3 nm after the comb copolymers are detached and we included approximate corrections to subtract the contribution by the remaining charge separation (dashed lines in Figure 9a-c).

Entropy has been suggested to drive the adsorption of PCEs to cement surfaces in experiments.<sup>87</sup> The simulation results indicate by the difference between free energies and energies of adsorption ( $\Delta G = \Delta H - T\Delta S$ ), at the scale of single polymer molecules, that entropic driving

forces can be significant for PCEs with a small fraction of side chains on C-S-H surface environments with strong water ordering, such as (100) surfaces of tobermorite 14 Å at pH ~12. A large entropy contribution to binding does not appear to be present for all C-S-H surface environments and for PCEs with a high fraction of side chains. The role of entropy for the adsorption and assembly of polymer films at higher coverage as used in experiment remains an open question (see further discussion in Section S4 in the ESI).

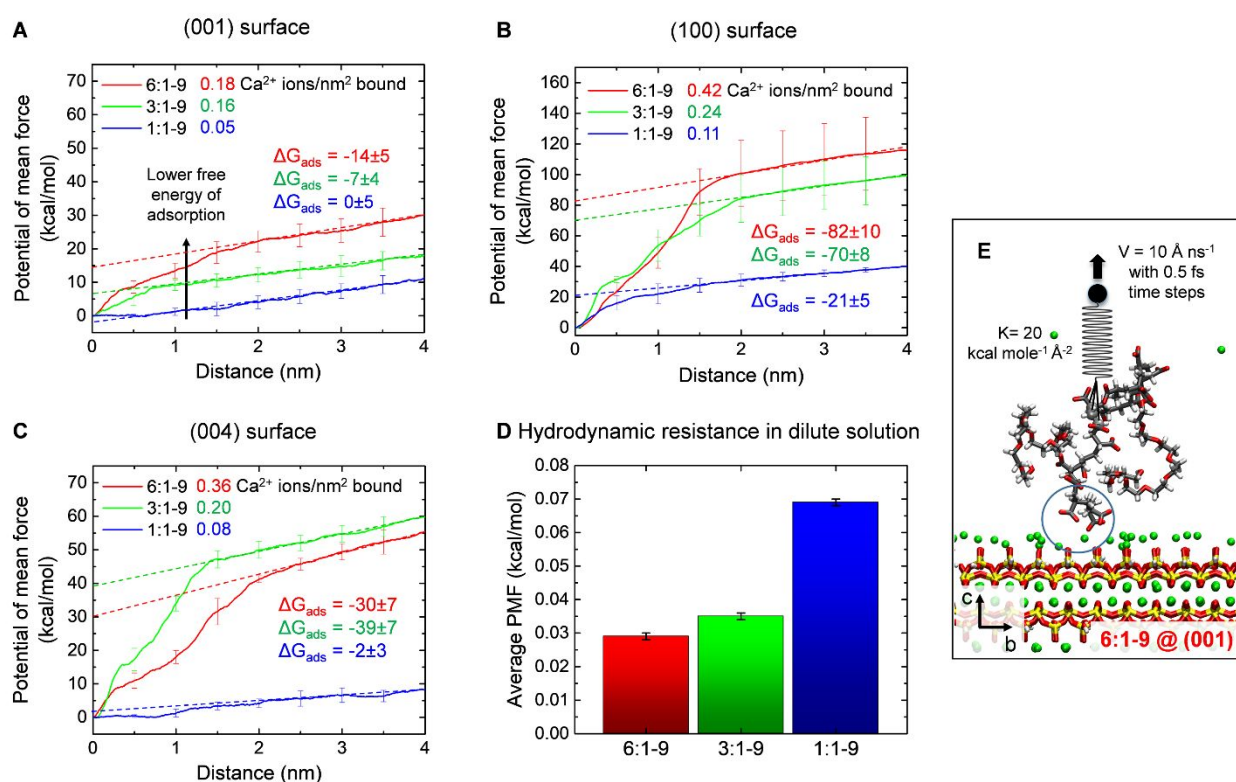


**Figure 9.** Free energy of binding of PCEs with 9mer PEG side chains to the C-S-H model surfaces according to steered molecular dynamics simulation. Several calcium ions from the PCEs remain bound to the surface (numbers in color, top) and free energies of binding are estimated after corrections for the remaining distance-dependence of the free energy ( $\Delta G_{\text{ads}}$ , dashed lines). (a) Potential of mean force (free energy) of PCE desorption as a function of distance from the (001)

surface of tobermorite 14 Å. (b) Free energy profile of PCE desorption on the (100) surface. The COO<sup>-</sup> side groups in PCEs 6:1-9 and 3:1-9 are more tightly bound and displace more surface-bound water molecules compared to other surfaces. Nearly all Ca<sup>2+</sup> ions remain bound to the surface. (c) Free energy profile of PCE desorption on the (004) surface. (d) The hydrodynamic work associated with the motion of the PCEs through the aqueous solution is negligible. (e) Setup of steered MD simulations. The center of the polymer backbone was pulled away from the surface. Successive COO<sup>-</sup> groups in the backbone compete for adsorption on the surface up to ~1.5 nm distance (blue circle). Free energies of adsorption tend to be equal or larger negative values relative to energies of adsorption, corresponding to a negligible or positive entropy of adsorption.

**Effect of Added Electrolytes and Higher PCE Surface Coverage.** The role of added electrolytes was tested for a concentration of Ca(OH)<sub>2</sub> of 0.2 M, which is at the high end of ionic concentrations in pore solutions (Figure 10a-d).<sup>58, 59</sup> The adsorption mechanism of the PCEs remains the same. However, the added ions occupy available surface sites and diminish the strength of adsorption. A reduction in energy and free energy of adsorption is similar within the uncertainty, on the order of 10 to 20 kcal/mol, for the examples of PCEs 6:1-9 and 1:1-3 on the (100) tobermorite 14 Å surfaces. Lower concentrations of ~0.1 M would likely show less significant effects. We also tested the average binding energy of an amorphous Ca(OH)<sub>2</sub> layer on top of the tobermorite surface, using initially supersaturated solutions up to 0.6 M Ca(OH)<sub>2</sub> (Figure S8 in the ESI). The resulting binding energies between -2 and -3 kcal per mol Ca(OH)<sub>2</sub> show that growth of portlandite tends to be favorable over adsorption of the PCEs (between 0 and -3 kcal per mol monomer), albeit of a similar magnitude. Follow-on studies could provide interesting details

on the influence of  $\text{Na}^+$ ,  $\text{K}^+$ ,  $\text{Ca}^{2+}$ ,  $\text{Mg}^{2+}$ ,  $\text{SO}_4^{2-}$ ,  $\text{Cl}^-$ ,  $\text{OH}^-$ , and aluminate ions for a range of relevant concentrations in pore solutions.<sup>58, 59</sup>

Comparisons with the typical dosage of PCEs in cement formulations will require simulations with surface coverage up to 10 times higher than investigated here for single molecules. Preliminary data for multiple PCE molecules indicate association with each other via  $\text{Ca}^{2+}$  ions between ionic groups of neighbor backbones (Figure 10e, f). As shown for PCE 6:1-9, the presence of ionic backbones can stabilize tilted orientations (Figure 10e) while flat-on conformations are disfavored (Figure 10f). Acrylate backbones with significant negative charge also experience repulsion and do not associate with each other in dilute solution away from the surface. Side-by-side conformations of PCEs with trapped  $\text{Ca}^{2+}$  ions in between the negatively charged backbones could increase the adsorbed mass per unit area to values in experiments (2 to 8 mg PCE per g of cement).<sup>83, 87, 91</sup> Packing in such cohesive, continuous polymer films may slow down diffusion of water onto the C-S-H surface and associated hydration reactions.

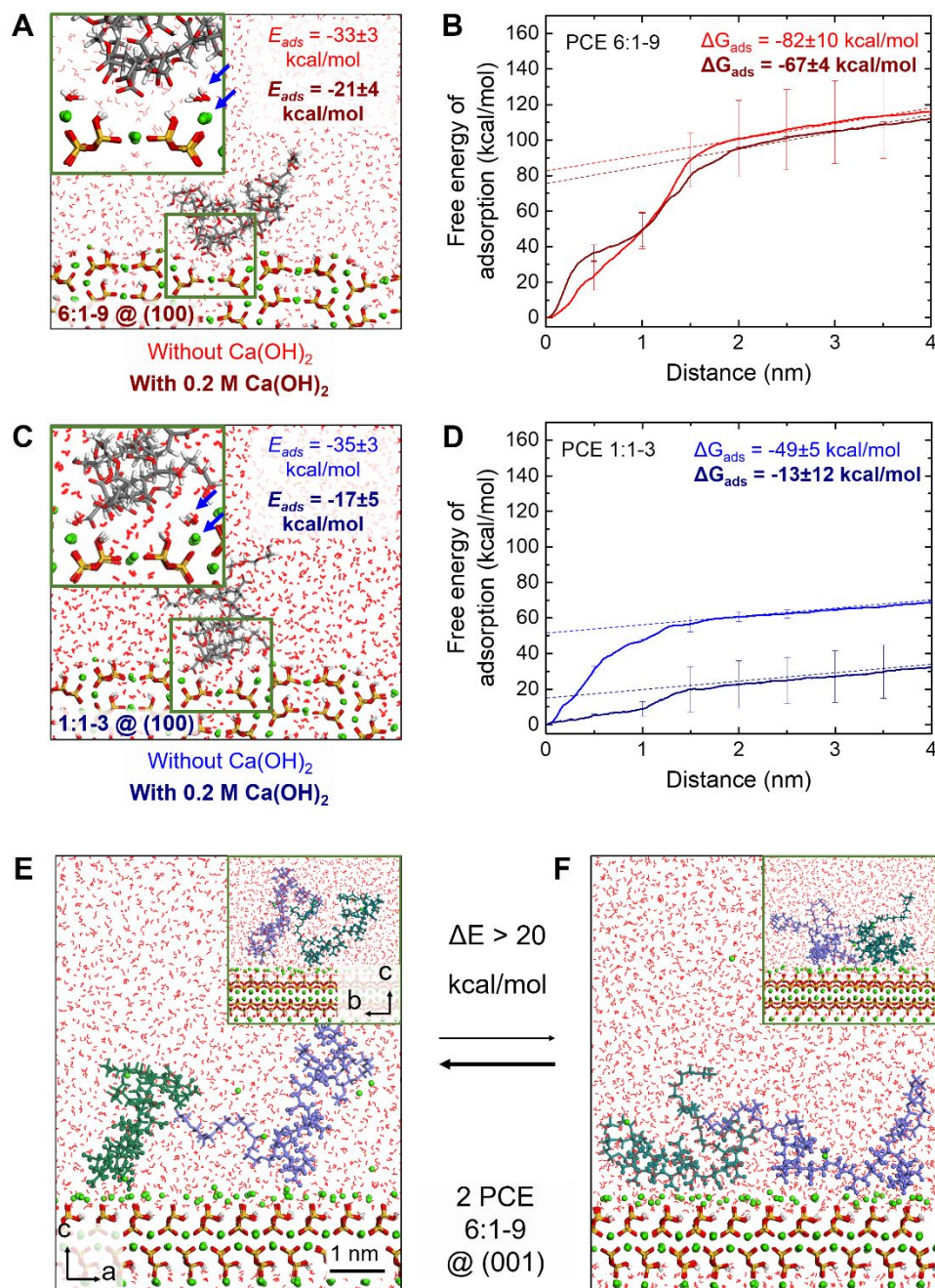


**Figure 10.** Effect of added electrolytes (0.2 mol/l  $\text{Ca}(\text{OH})_2$ ) and increased surface coverage with PCEs on binding of the comb-copolymers. (a-d) Adsorbed conformations and binding energies of PCEs 6:1-9 and 1:1-3 on the (100) surface of tobermorite 14 Å in the presence of 0.2 mol/l  $\text{Ca}(\text{OH})_2$  in the pore solution. The added electrolyte sustains the principal PCE adsorption mechanism and reduces the energy and free energy of adsorption of the PCEs. Additional  $\text{Ca}^{2+}$

ions in the solution occupy available under-coordinated surface sites that are otherwise targeted by  $\text{Ca}^{2+}$  ions from the PCE, and  $\text{OH}^-$  ions coordinate calcium ions on the surface that reduce the accessibility and binding by carboxylate groups (see blue arrows in insets in a and c). These competing effects explain an overall decrease in binding affinity of the PCEs. Reductions in the energy and in the free energy of adsorption are similar for the two example systems within the uncertainty. The free energy curves are an average over multiple independent simulations by steered molecular dynamics. (e, f) Effect of higher surface coverage on conformations of PCE 6:1-9 molecules on the (001) surface. Three oligomers were included of which one remained in solution. A side-by-side tilted orientation of the backbones stabilized by  $\text{Ca}^{2+}$  ion bridges was preferred (e). Alternative, flat-on conformations (f) had a significantly higher average energy due to conformation strain. The insets show the same adsorbed conformation from a different viewing angle. The contact time of each oligomer was <100% in all conformations.

**Further Comparison with Experimental Measurements.** The sensitivity of PCE adsorption to surface binding sites has been noticed in experiments.<sup>12, 20</sup> Experiments with non-reactive surfaces concluded that a higher positive surface charge results in stronger PCE adsorption,<sup>82</sup> supporting the proposed adsorption mechanism. Quantitative adhesion measurements of PCEs on C-S-H surfaces have not yet been reported. However, data by atomic force microscopy (AFM) and calorimetry suggest adsorption energies of a few  $RT$  per acrylate monomer, i.e., several times  $-0.6$  kcal/mol at room temperature (e.g. PCE S3 which corresponds to PCE 2.3:1-23 with DP = 83).<sup>92</sup> The computed adsorption energies on surfaces at pH  $\sim 12$  and for longer PEG chains are between  $-10$  and  $-49$  kcal/mol per 16mer of PCE, equal to a range of  $-0.6$  and  $-3.0$  kcal per mol acrylate monomer (Figure 8a-c). The simulation data are thus in an expected range according to

experiments for comparable surface coverage. However, it remains challenging to verify equal surface chemistry and electrolyte composition. Prior simulations of other, better defined organic-inorganic interfaces with IFF have shown agreement of computed and experimental adsorption data within  $\pm 10\%$ .<sup>29, 31, 36, 37, 77, 90, 93</sup>

Longer PCE backbones of 4:1-z topology were reported to increase the adsorbed mass at the same mass concentration.<sup>26, 94</sup> Such cumulative addition of binding strength by a larger number of acrylate groups supports the proposed mechanism of ion pairing (Figures 4 and 7a) and possibly the formation of tilted conformations with increased inter-chain interactions (Figure 10e, f). Experimental data have also shown that PCEs with a high density of longer side chains exhibit a lower adsorbed mass.<sup>95</sup> The simulation results, albeit at lower surface coverage, indicate less surface contact in these cases (PCE 1:1-9 in Figure 6a, d, g) as well as weaker adsorption energies (Figure 8a-c).

PEG side chains likely support better particle dispersion by steric stabilization of the surfaces.<sup>12, 96, 97</sup> A common cartoon depicts flat-on backbone conformations with side chains pointing into the solution (similar to Figure 6d). The simulations show, however, that typical conformations for lower density of side chains look different. Hydrophilic PEG side chains in the interfacial region on the surface of the particles may support dispersion, however, they do not hinder the access of water to the particle surface. Tilted and irregular conformations of the backbone (Figure 5c, f, i, Figure 6c, f, i, Figure S1c, f, i), and side-by-side stacking of PCEs through ionic interactions (Figure 10e, f), controlled by the density and length of PEG side chains, may lead to a thicker film and delay hydration reactions.<sup>98</sup> In this manner, packing of multiple PCEs backbones with higher molecular weight and a low density of PEG side chains could explain

experimental observations of higher adsorbed mass, increased barriers to hydration, and longer hydration time.<sup>99</sup>

The poly(acrylic acid) backbones investigated here likely increase conformation flexibility and surface coverage by a small amount in comparison to poly(methacrylic acid) backbones. The absence of  $-\text{CH}_3$  side groups and increased alkaline hydrolysis, which results in loss of PEG side chains over time, have shown increased cement fluidity for the same adsorbed mass in experiments.<sup>79</sup>

Diverse observations have been reported for zeta potentials. Some experimental studies report a small negative zeta potential (-) of cement particles upon addition of PCEs that increases and sometimes reverses to positive values (+).<sup>95, 100</sup> However, also positive zeta potentials and a decrease to negative values upon addition of PCEs have been reported.<sup>11, 82</sup> The opposing trends, (+) or (-), are likely related to the dissociation and association of different ions on the particle surface under exposure to an electric field. Scenarios may include, for example, dissociation of calcium ions from superficial silicate ions on a C-S-H surface (-), of hydroxide ions from superficial calcium hydroxide layers (+), of PCEs from added superficial calcium ions on a C-S-H surface (+), and of calcium ions from dense surface-adsorbed PCE multilayer films (-). The presence of ions with less affinity to the surface such as  $\text{Na}^+$  or  $\text{K}^+$  ions used in some PCE formulations may also play a role (see details in section S5 in the ESI).

The data show that understanding of the complex working mechanisms at higher surface coverage<sup>1, 9, 11, 101, 102</sup> critically depends on advances in experimental imaging and on further guidance by computational methods. Current limitations and opportunities are discussed in Section S6 in the ESI.

## Conclusions

Our study is the first systematic and quantitative analysis of comb copolymer interactions with calcium silicate hydrate minerals at the single molecule scale and lays a foundation for understanding their working mechanism, rational design, and improvement of sustainable building materials. We investigated a series of widely used polycarboxylate ethers (PCEs) in contact with calcium-silicate-hydrate surfaces using molecular dynamics simulations and comparisons to available experimental data. The surfaces were represented by well-defined (h k l) cleavage planes of tobermorite 14 Å that mimic possible surface environments, typical solution conditions from pH 10 to 14. No further electrolytes were added for simplicity, except for specific test cases.

Under these conditions, calcium ions pertaining to the negatively charged acrylate backbone migrate to the cement-water interface and adsorb onto under-coordinated surface sites of the calcium silicate hydrate (C-S-H) gel. Motion of the comb copolymer to the surface follows, whereby anionic carboxylate groups coordinate existing and newly adsorbed calcium ions on the silicate surface. Polyethylene oxide (PEO) side chains avoid contact with the C-S-H surface and remain solvated by water.

All PCE binding energies were in the attractive range of -0.20 to -3.1 kcal/mol, and the binding free energies amount to between 0 and -5 kcal/mol, respectively. Computed binding free energies are overall similar to binding energies, although binding free energies can assume larger negative values due to the release of more surface-bound water molecules and a net entropy gain. The binding strength primarily scales with the calcium-to-silicate ratio of the surface (C/S ratio), showing more than twice the adsorption energy as the surface C/S ratio increases from 0.5 to 1.0. Then, carboxylate groups in the PCEs can coordinate calcium ions on the mineral surface. The binding strength and conformations are further controlled by the density and length of PEG side

chains. The binding strength increases for lower degree of esterification and longer side chains (PCEs 6:1-9 and 3:1-9). The binding strength is also significant for high degree of esterification and short side chains, although the contact time then remains less than 100% (PCE 1:1-3). Up to two successive  $\text{COO}^-$  side groups on the acrylate backbone can bind next to each other on the surface, and further consecutive carboxylate groups lead to detachment of part of the backbone due to electrostatic repulsion and conformation strain. Esterified groups in between anionic groups assist the backbone in re-gaining contact with the surface. The addition of electrolytes such as  $\text{Ca}(\text{OH})_2$  introduces competition for surface sites for adsorption and tends to reduce PCE adsorption without changing the principal interaction mechanism.

Typically, flat-on binding occurs in the presence of more side chains (PCEs 1:1-z) and tilted, more flexible and stronger binding in the presence of fewer side chains (PCEs 6:1-z). A larger density of side chains increases the selectivity to a particular (hkl) surface environment due to less conformational flexibility, yet also decreases the contact time and binding strength. The presence of multiple oligomers with low density of side chains shows a preference for tilted orientations on the surface over flat-on orientations, which may help in the formation of cohesive polymer films, higher adsorbed mass, and delay in hydration observed in experiment.

The binding mechanism is consistent with experimental observations and the data allow the interpretation of known qualitative trends in surface-selective binding, the role of the density of ionic side chains in the oligomers, adsorption energies, temperature, and zeta potential measurements from the atomic scale. The computational results may be specifically tested in future experimental studies as imaging and spectroscopy techniques advance. As an approximation, we do not consider the range of electrolytes present in pore solutions and higher surface coverage with continuous polymer films. Follow-on studies will be helpful to examine the influence of

amorphous C-S-H morphologies in comparison to well-defined tobermorite 14 Å cleavage planes, various ions, the assembly and stability of polymer films on C-S-H surfaces, as well as the role of polydispersity of the polymer molecular weight. The reported mechanisms can also serve as a starting point to understand the interaction of the PCEs with other calcium minerals, for example, aluminates and sulfates in cement, as well as apatites, carbonates, and sulfates in biomaterials.

### Acknowledgment

This work was supported by the Petroleum Research Fund of the American Chemical Society (ACS-PRF 54135-ND10), the National Science Foundation (CBET 1530790, OAC 1931587), and the University of Colorado at Boulder. The allocation of computational resources at the CU Biofrontiers Computing Cluster and at the Ohio Supercomputing Center is acknowledged. This work further used resources of the Oak Ridge Leadership Computing Facility at the Oak Ridge National Laboratory, which is supported by the Office of Science of the U.S. Department of Energy under Contract No. DE-AC05-00OR22725, the Argonne Leadership Computing Facility, which is a DOE Office of Science User Facility supported under Contract DE-AC02-06CH11357, and the Janus supercomputer, which is supported by the National Science Foundation (award number CNS-0821794).

### References

1. P. C. Aitcin and R. J. Flatt, eds., *Science and Technology of Concrete Admixtures*, Woodhead Publishing, Amsterdam, 2015.
2. K. L. Scrivener and A. Nonat, *Cem. Concr. Res.*, 2011, **41**, 651-665.
3. H. F. W. Taylor, *Cement Chemistry*, Thomas Telford, 1997.
4. R. Kajaste and M. Hurme, *J. Cleaner Prod.*, 2016, **112**, 4041-4052.
5. H. Mikulcic, J. J. Klemes, M. Vujanovic, K. Urbaniec and N. Duic, *J. Cleaner Prod.*, 2016, **136**, 119-132.

6. B. Lothenbach, K. Scrivener and R. Hooton, *Cem. Concr. Res.*, 2011, **41**, 1244-1256.
7. K. L. Scrivener, *Indian Concr. J.*, 2014, **88**, 11-21.
8. B. C. McLellan, R. P. Williams, J. Lay, A. van Riessen and G. D. Corder, *J. Cleaner Prod.*, 2011, **19**, 1080-1090.
9. F. Dalas, S. Pourchet, A. Nonat, D. Rinaldi, S. Sabio and M. Mosquet, *Cem. Concr. Res.*, 2015, **71**, 115-123.
10. J. Plank, K. Poellmann, N. Zouaoui, P. R. Andres and C. Schaefer, *Cem. Concr. Res.*, 2008, **38**, 1210-1216.
11. O. Akhlaghi, Y. Z. Menciloglu and O. Akbulut, *Sci. Rep.*, 2017, **7**, 41743.
12. D. Marchon, U. Sulser, A. Eberhardt and R. J. Flatt, *Soft Matter*, 2013, **9**, 10719-10728.
13. K. Yoshioka, E. Sakai, M. Daimon and A. Kitahara, *J. Am. Ceram. Soc.*, 1997, **80**, 2667-2671.
14. R. K. Mishra, R. J. Flatt and H. Heinz, *J. Phys. Chem. C*, 2013, **117**, 10417-10432.
15. P. J. M. Smeets, K. R. Cho, R. G. E. Kempen, N. Sommerdijk and J. J. De Yoreo, *Nat. Mater.*, 2015, **14**, 394-399.
16. H. Heinz, C. Pramanik, O. Heinz, Y. Ding, R. K. Mishra, D. Marchon, R. J. Flatt, I. Estrela-Lopis, J. Llop, S. Moya and R. F. Ziolo, *Surf. Sci. Rep.*, 2017, **72**, 1-58.
17. M. J. Rosen, *J. Am. Oil Chem. Soc.*, 1975, **52**, 431-435.
18. M. Turesson, C. Labbez and A. Nonat, *Langmuir*, 2011, **27**, 13572-13581.
19. C. Giraudeau, J. B. D. de Lacaillerie, Z. Souguir, A. Nonat and R. J. Flatt, *J. Am. Ceram. Soc.*, 2009, **92**, 2471-2488.
20. D. Marchon, P. Juilland, E. Gallucci, L. Frunz and R. J. Flatt, *J. Am. Ceram. Soc.*, 2017, **100**, 817-841.
21. S. Mantellato, M. Palacios and R. J. Flatt, *Cem. Concr. Res.*, 2015, **67**, 286-291.
22. P. C. Aitcin and R. J. Flatt, *Science and Technology of Concrete Admixtures*, Elsevier Science, 2015.
23. K. L. Scrivener, P. Juilland and P. J. M. Monteiro, *Cem. Concr. Res.*, 2015, **78**, 38-56.
24. J. Cheung, A. Jeknavorian, L. Roberts and D. Silva, *Cem. Concr. Res.*, 2011, **41**, 1289-1309.
25. R. Flatt and I. Schober, in *Understanding the Rheology of Concrete*, ed. N. Roussel, Woodhead Publishing, 2012, DOI: <http://dx.doi.org/10.1533/9780857095282.2.144>, pp. 144-208.
26. F. Winnefeld, S. Becker, J. Pakusch and T. Götz, *Cem. Concr. Compos.*, 2007, **29**, 251-262.
27. Q. Ran, P. Somasundaran, C. Miao, J. Liu, S. Wu and J. Shen, *J. Colloid Interface Sci.*, 2009, **336**, 624-633.
28. K. Yamada, T. Takahashi, S. Hanehara and M. Matsuhisa, *Cem. Concr. Res.*, 2000, **30**, 197-207.
29. I. L. Geada, H. Ramezani-Dakhel, T. Jamil, M. Sulpizi and H. Heinz, *Nat. Commun.*, 2018, **9**, 716.
30. X. Shu, Q. Ran, J. Liu, H. Zhao, Q. Zhang, X. Wang, Y. Yang and J. Liu, *Constr. Build. Mater.*, 2016, **116**, 289-298.
31. H. Heinz, T.-J. Lin, R. K. Mishra and F. S. Emami, *Langmuir*, 2013, **29**, 1754-1765.
32. R. K. Mishra, A. K. Mohamed, D. Geissbühler, H. Manzano, T. Jamil, R. Shahsavari, A. G. Kalinichev, S. Galmarini, L. Tao, H. Heinz, R. Pellenq, A. C. T. van Duin, S. C. Parker, R. J. Flatt and P. Bowen, *Cem. Concr. Res.*, 2017, **102**, 68-89.
33. E. Bonaccorsi, S. Merlino and A. R. Kampf, *J. Am. Ceram. Soc.*, 2005, **88**, 505-512.
34. H. Heinz and H. Ramezani-Dakhel, *Chem. Soc. Rev.*, 2016, **45**, 412-448.
35. E. Pustovgar, R. K. Mishra, M. Palacios, J. B. d'Espinose de Lacaillerie, T. Matschei, A. S. Andreev, H. Heinz, R. Verel and R. J. Flatt, *Cem. Concr. Res.*, 2017, **100**, 245-262.
36. F. S. Emami, V. Puddu, R. J. Berry, V. Varshney, S. V. Patwardhan, C. C. Perry and H. Heinz, *Chem. Mater.*, 2014, **26**, 5725-5734.
37. S. V. Patwardhan, F. S. Emami, R. J. Berry, S. E. Jones, R. R. Naik, O. Deschaume, H. Heinz and C. C. Perry, *J. Am. Chem. Soc.*, 2012, **134**, 6244-6256.
38. C. C. Dharmawardhana, K. Kanhaiya, T.-J. Lin, A. Garley, M. R. Knecht, J. Zhou, J. Miao and H. Heinz, *Mol. Sim.*, 2017, **43**, 1394-1405.

39. C. Pramanik, J. R. Gissinger, S. Kumar and H. Heinz, *Acs Nano*, 2017, **11**, 12805-12816.
40. Y. Zhou, D. Hou, H. Manzano, C. A. Orozco, G. Geng, P. J. M. Monteiro and J. Liu, *ACS Appl. Mater. Interfaces*, 2017, **9**, 41014-41025.
41. R. Shahsavari, R. J. M. Pellenq and F. J. Ulm, *Phys. Chem. Chem. Phys.*, 2011, **13**, 1002-1011.
42. H. Heinz and U. W. Suter, *J. Phys. Chem. B*, 2004, **108**, 18341-18352.
43. R. J. Pellenq, A. Kushima, R. Shahsavari, K. J. Van Vliet, M. J. Buehler, S. Yip and F. J. Ulm, *Proc. Natl. Acad. Sci. U. S. A.*, 2009, **106**, 16102-16107.
44. R. K. Mishra, D. Geissbuhler, H. A. Carmona, F. K. Wittel, M. L. Sawley, M. Weibel, E. Gallucci, H. J. Herrmann, H. Heinz and R. J. Flatt, *Adv. Appl. Ceram.*, 2015, **114**, 393-401.
45. R. K. Mishra, H. Heinz, T. Müller, J. Zimmermann and R. J. Flatt, *American Concrete Institute Symposium Series*, 2012, **288**, 235-251.
46. R. K. Mishra, M. Weibel, T. Muller, H. Heinz and R. J. Flatt, *Chimia*, 2017, **71**, 451-460.
47. Y. T. Fu and H. Heinz, *Chem. Mater.*, 2010, **22**, 1595-1605.
48. R. K. Mishra, L. Fernández-Carrasco, R. J. Flatt and H. Heinz, *Dalton Trans.*, 2014, **43**, 10602-10616.
49. H. Heinz, H. Koerner, K. L. Anderson, R. A. Vaia and B. L. Farmer, *Chem. Mater.*, 2005, **17**, 5658-5669.
50. T. Hirata, P. Branicio, J. Ye, J. W. Zheng, Y. Tomike, A. Lange, J. Plank and M. Sullivan, *Adv. Cem. Res.*, 2017, **29**, 418-428.
51. Q. Ran, H. Zhao, X. Shu, Q. Zhang, Y. Yang, J. Liu and S. Wu, *Comput. Mater. Sci.*, 2015, **109**, 90-96.
52. T. Hirata, J. Ye, P. Branicio, J. W. Zheng, A. Lange, J. Plank and M. Sullivan, *Sci. Rep.*, 2017, **7**, 16599.
53. H. X. Zhao, Y. W. Wang, Y. Yang, X. Shu, H. Yan and Q. P. Ran, *Appl. Surf. Sci.*, 2017, **407**, 8-15.
54. M. Turesson, A. Nonat and C. Labbez, *Langmuir*, 2014, **30**, 6713-6720.
55. A. Picker, L. Nicoleau, Z. Burghard, J. Bill, I. Zlotnikov, C. Labbez, A. Nonat and H. Cölfen, *Sci. Adv.*, 2017, **3**, e1701216.
56. *Interface Force Field (IFF) and a Surface Model Database*, <https://bionanostructures.com/interface-md/>. 2013-2019.
57. F. S. Emami, V. Puddu, R. J. Berry, V. Varshney, S. V. Patwardhan, C. C. Perry and H. Heinz, *Chem. Mater.*, 2014, **26**, 2647-2658.
58. B. Lothenbach, F. Winnefeld and R. Figi, presented in part at the 12th International Congress on the Chemistry of Cement, Montreal, Canada, 2007.
59. D. Bonen and S. L. Sarkar, *Cem. Concr. Res.*, 1995, **25**, 1423-1434.
60. R. J. Stewart, S. Goyal, S. H. Lee, A. Rammohan, H. H. Park, K. Min, E. Cho and H. Heinz, *J. Chem. Phys.*, 2019, **150**, 174703.
61. H. Heinz, *J. Phys.: Condens. Matter*, 2014, **26**, 244105.
62. H. Heinz, *Curr. Opin. Chem. Eng.*, 2016, **11**, 34-41.
63. T. Jamil, J. R. Gissinger, A. Garley, N. Saikia, A. Upadhyay and H. Heinz, *Nanoscale*, 2019, **11**, 11183-11194.
64. A. Garley, S. E. Hoff, N. Saikia, S. N. Jamadagni, A. A. Baig and H. Heinz, *J. Phys. Chem. C*, 2019, **123**, 16982-16993.
65. T. Z. Lin and H. Heinz, *J. Phys. Chem. C*, 2016, **120**, 4975-4992.
66. S. Merlino, E. Bonaccorsi and T. Armbruster, *Eur. J. Mineral.*, 2001, **13**, 577-590.
67. S. A. Hamid, *Z Kristallographie*, 1981, **154**, 189-198.
68. D. R. Lide, *CRC Handbook of Chemistry and Physics* CRC Press, Boca Raton, FL, 96th edn., 2015.
69. S. Brunauer, D. L. Kantro and C. H. Weise, *Can. J. Chem.*, 1959, **37**, 714-724.
70. K. Haraguchi and H.-J. Li, *Macromolecules*, 2006, **39**, 1898-1905.
71. J. Wu, J. Lin, M. Zhou and C. Wei, *Macromol. Rapid Commun.*, 2000, **21**, 1032-1034.
72. H. Heinz, *Clay Miner.*, 2012, **47**, 205-230.

73. C. Pramanik, T. Jamil, J. R. Gissinger, D. Guittet, P. J. Arias-Monje, S. Kumar and H. Heinz, *Adv. Funct. Mater.*, 2019, **29**, 1905247.
74. S. Kobayashi and K. Müllen, *Encyclopedia of Polymeric Nanomaterials*, Springer Berlin Heidelberg.
75. H. Heinz, R. A. Vaia, R. Krishnamoorti and B. L. Farmer, *Chem. Mater.*, 2007, **19**, 59-68.
76. L. Y. Ruan, H. Ramezani-Dakhel, C. Lee, Y. J. Li, X. F. Duan, H. Heinz and Y. Huang, *Acs Nano*, 2014, **8**, 6934-6944.
77. J. Feng, J. M. Slocik, M. Sarikaya, R. R. Naik, B. L. Farmer and H. Heinz, *Small*, 2012, **8**, 1049-1059.
78. J. Plank, K. Pöllmann, N. Zouaoui, P. R. Andres and C. Schaefer, *Cem. Concr. Res.*, 2008, **38**, 1210-1216.
79. A. Lange and J. Plank, *J. Appl. Polym. Sci.*, 2015, **132**, 42529.
80. G. W. Gokel, W. M. Leevy and M. E. Weber, *Chem. Rev.*, 2004, **104**, 2723-2750.
81. A. Zingg, F. Winnefeld, L. Holzer, J. Pakusch, S. Becker and L. Gauckler, *J. Colloid Interface Sci.*, 2008, **323**, 301-312.
82. L. Ferrari, J. Kaufmann, F. Winnefeld and J. Plank, *J. Colloid Interface Sci.*, 2010, **347**, 15-24.
83. Q. P. Ran, P. Somasundaran, C. W. Miao, J. P. Liu, S. S. Wu and J. Shen, *J. Dispersion Sci. Technol.*, 2010, **31**, 790-798.
84. A. Kulbida, M. N. Ramos, M. Rasanen, J. Nieminen, O. Schrems and R. Fausto, *J. Chem. Soc. Faraday Trans.*, 1995, **91**, 1571-1585.
85. W. A. Herrebout, B. J. Vanderveken, A. Wang and J. R. Durig, *J. Phys. Chem.*, 1995, **99**, 578-585.
86. H. Taylor, P. Barret, P. Brown, D. Double, G. Frohnsdorff, V. Johansen, D. Ménétrier-Sorrentino, I. Odler, L. Parrott and J. Pommersheim, *Mat. Constr.*, 1984, **17**, 457-468.
87. J. Plank, B. Sachsenhauser and J. de Reese, *Cem. Concr. Res.*, 2010, **40**, 699-709.
88. C. Jarzynski, *Phys. Rev. Lett.*, 1996, **78**, 2690-2693.
89. S. Park, F. Khalili-Araghi, E. Tajkhorshid and K. Schulten, *J. Chem. Phys.*, 2003, **119**, 3559-3566.
90. H. Ramezani-Dakhel, L. Y. Ruan, Y. Huang and H. Heinz, *Adv. Funct. Mater.*, 2015, **25**, 1374-1384.
91. A. Lange and J. Plank, *Cem. Concr. Res.*, 2016, **79**, 131-136.
92. R. J. Flatt, I. Schober, E. Raphael, C. Plassard and E. Lesniewska, *Langmuir*, 2009, **25**, 845-855.
93. M. Schneemilch and N. Quirke, *Chem. Phys. Lett.*, 2016, **664**, 199-204.
94. X. Wang, Q. Ran, Y. Yang and X. Shu, *Adv. Cem. Res.*, 2016, **28**, 371-377.
95. A. Zingg, F. Winnefeld, L. Holzer, J. Pakusch, S. Becker, R. Figi and L. Gauckler, *Cem. Concr. Compos.*, 2009, **31**, 153-162.
96. M. Shonaka, K. Kitagawa and H. Satoh, *Special Publication*, 1997, **173**, 599-614.
97. Y. L. Yaphary, R. H. W. Lam and D. Lau, *Procedia Engineering*, 2017, **172**, 1270-1277.
98. P. Juilland, L. Nicoleau, R. S. Arvidson and E. Gallucci, *RILEM Techn. Lett.*, 2017, **2**, 90-98.
99. F.-r. Kong, L.-s. Pan, C.-m. Wang and N. Xu, *Constr. Build. Mater.*, 2016, **105**, 545-553.
100. S. R. Plank J, Vlad D, Brandl A, Chatziagorastou P., *GDCh-Monographie Band*, 2004, **31**, 58-69.
101. S. Pourchet, C. Comparet, L. Nicoleau and A. Nonat, Influence of PC Superplasticizers on Tricalcium Silicate Hydration, In *12th International Congress on the Chemistry of Cement - ICCC 2007*, Montreal, Canada, 2007.
102. F. Dalas, A. Nonat, S. Pourchet, M. Mosquet, D. Rinaldi and S. Sabio, *Cem. Concr. Res.*, 2015, **67**, 21-30.